Ductile rupture of 2024 aluminum thin sheets – Experimental study of damage growth and crack initiation.

F. Bron[1,2], J. Besson[1], A. Pineau[1] and J.-C. Ehrström[2]

[1]Centre des Matériaux, ENSMP, BP 87, 91003 Evry Cedex, France
[2]Pechiney Centre de Recherches de Voreppe, BP 27, 38341 Voreppe Cedex, France

ABSTRACT: *The damage and rupture mechanisms of a 2024 aluminum thin sheet are investigated. Mechanical tests are carried out on flat specimens including smooth tensile panels, U-notched samples with various notch radii and V-notched samples. Cracked samples were also tested which include Kahn samples and large MT panels; stable crack growth is obtained in both cases. The microstructure of the material is characterized to obtain the second phase volume content. The largest particles consist of intermetallics. The macroscopic fracture surface of the different specimens is observed using scanning electron microscopy. Smooth and moderately notched samples exhibit a slanted fracture surface, which has an angle of about 45° with the loading direction. With increasing notch severity, the fracture mode changes significantly. Failure initiates at the notch root in a small triangular region whose normal is parallel to the loading direction. Outside this zone, slant fracture is observed. Microscopic observations show two failure mechanisms. Voids are first initiated at intermetallics in both cases. At low stress triaxiality ratio (smooth or moderately notched samples), these voids tend to coalesce rapidly according to a "void sheet mechanism" which creates smaller dimples in the inter-void ligaments. At higher triaxiality, void growth is promoted and final rupture is caused by "internal necking" between the large cavities.*

INTRODUCTION

Alloys of the Al-Cu-Mg series, especially AA2024, show a good combination of static tensile properties, damage tolerance and formability. For this reason, they have been used for a long time in airframe structures, especially for fuselage skin. They are manufactured in the form of clad sheets, which exhibit a good corrosion resistance. The AA2024–T4 alloy studied below was developed by Pechiney Rhenalu. Its thickness is 1.75 mm and it is covered with a thin coat (less than 80 μm) of AA1050 (pure aluminum) on both faces.

This work is part of a wider project whose aim is the modeling of AA2024 fracture toughness. This project will be based on mechanical testing, metallographic observations and modeling. This paper addresses the first two points. Smooth, notched and cracked samples are used and fracture surfaces are observed in detail using scanning electron microscopy (SEM).

METALLURGICAL ANALYSIS

One of the major factors regarding damage tolerance is the presence of coarse second phase intermetallics and dispersoids. These phases are nucleation sites for damage beyond the crack tip during crack propagation. Thus, they are rather detrimental and must be avoided. The largest particles consist of intermetallics: AlCuFeMn and AlCuMg (figure 1.b). The first ones have an angular shape and a size of 5–15 μm. The second ones are round of diameter 2–3 μm. The phase volume fraction determined by image analysis is about 0.5 %. Dispersoids which are also present cannot be seen by optical microscopy. Figure 1.a shows that grains are almost equiaxed.

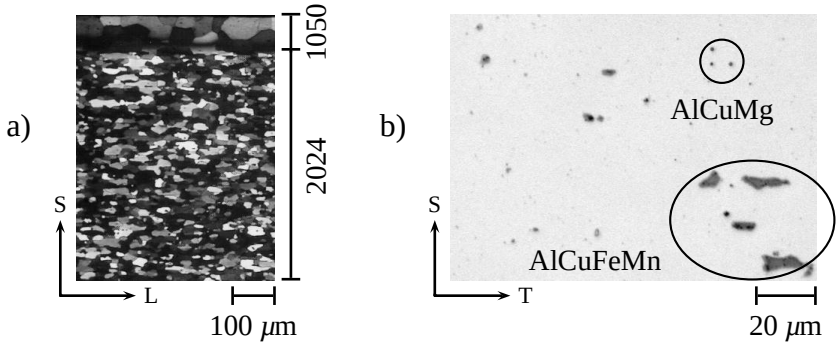

Figure 1: Microstructure of the AA2024 alloy – a) shows the grain shape in the L–S plane and b) shows intermetallic particles in the T–S plane (L stands for rolling direction, T for transverse direction and S for short transverse direction).

MECHANICAL TESTS

Seven types of samples have been used in this study (figure 2). MT760 samples are used to obtain a stable crack propagation over more than 100 mm. The standard R-curve test is used by aircraft manufacturers to qualify aluminum alloys [1]. However, this test is expensive and could be replaced by tests on small sized KA60 specimens [2] which also allow a stable crack propagation over more than 20 mm. The TR6 sample is a conventional smooth tensile specimen used to determine the elasto-plastic behavior. The differently notched samples EU05, EU1, EU2 and EV60 are used to access the behavior under various stress triaxiality ratios. The notch radius of KA60 and EV60 is less than 60 μm.

The mechanical properties have been determined with the TR6 specimens: the yield strength is about 320 MPa, the ultimate tensile strength 445 MPa, the homogeneous elongation 18 % and the fracture strain 23 %.

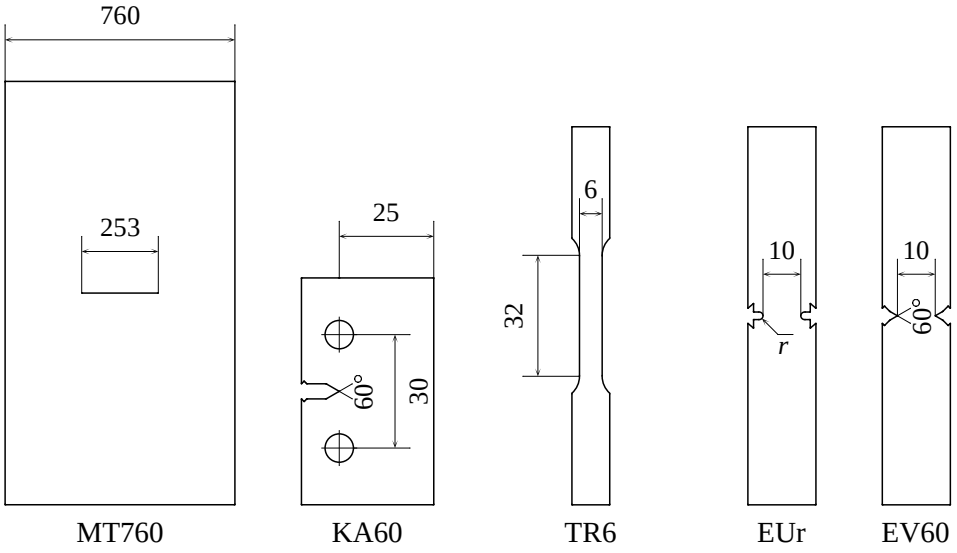

Figure 2: Specimens for mechanical tests (all dimensions in mm) – EUr = EU05, EU1 or EU2 with $r = 0.5$, 1 or 2 mm

ANALYSIS OF FRACTURE SURFACES

The rupture of all specimens is purely ductile: dimples of size 1–10 μm are observed.

Macroscopic fracture surface

The aspect of the fracture surface depends on the notch severity as shown in figure 3. MT760, KA60 and EV60 exhibit the same aspect: the crack begins with a flat triangle whose normal is parallel to the loading direction. This triangle has its base on the notch root and its height is about 1.5 times the sheet thickness. The remaining fracture surface is slanted with a 45 degrees angle with regard to the loading direction. When notch severity decreases (EU05), the triangle diminishes in size. Finally, for EU1, EU2 and TR6, there is no triangle at all and the whole surface is slanted. These results are the same as shown elsewhere [3].

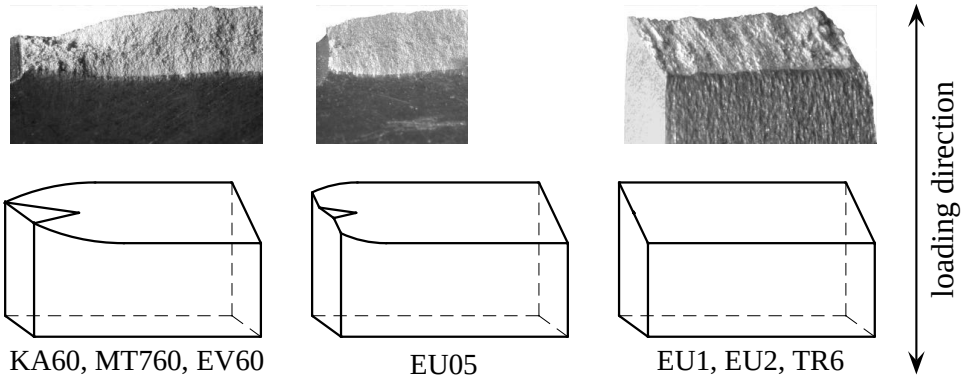

Figure 3: Shape of the fracture surface

Microscopic fracture surface

The aspect of the two regions defined above (the triangle and the slanted plane) are very different as shown in figure 4. In the first one, large dimples can be seen (10 μm) around large particles. Void growth has been dominant. In the second one, void growth is limited while very small secondary dimples (less than 1 μm) are also observed. The rupture surface also exhibits flat areas

where small dimples cannot be seen (cf. figure 5.a). This indicates that friction between both surfaces has occurred during the failure process as shown in figure 5.b.

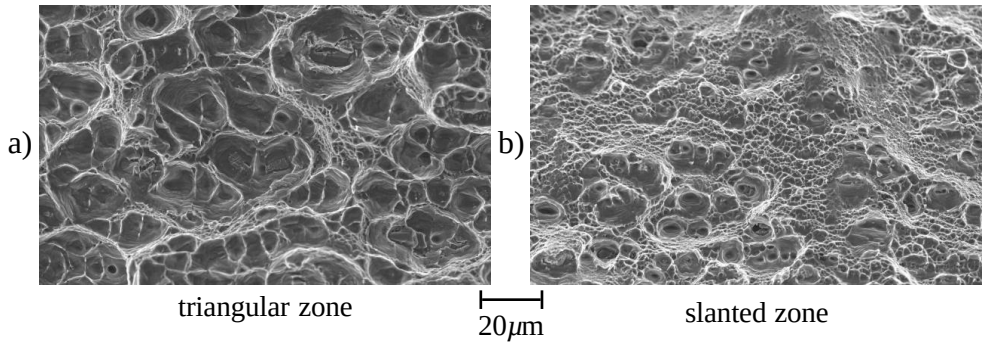

Figure 4: Aspect of both fracture zones

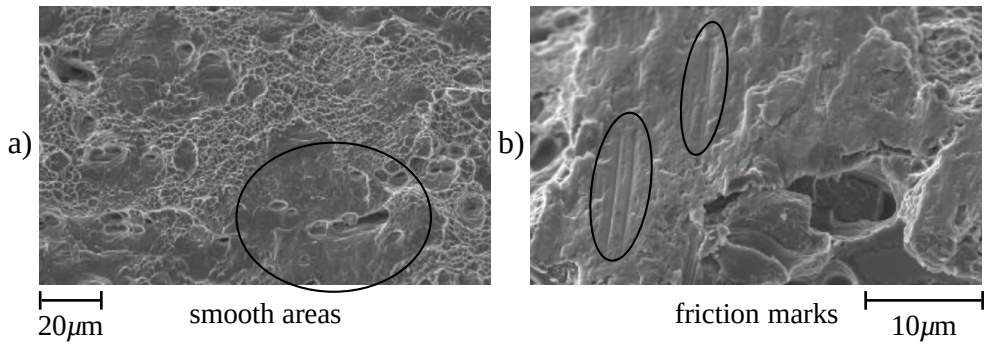

Figure 5: Smooth areas in the slanted zone and friction marks

Transition from flat to slanted crack path

To better understand the failure mechanism, interrupted tests were performed on KA60 samples in which stable crack growth is obtained. The load is decreased by 50 % when a given load-line displacement is obtained and the specimen is broken under fatigue. The fatigue facies is significantly different so it is rather easy to locate the crack front. Figure 6 shows the fracture aspect

of 5 interrupted tests. In this figure, successive positions of the crack front are shown. One notices that fracture is initiated well before the load maximum is reached in (b). It starts with the formation of a small flat triangular zone (a) whose normal is parallel to the loading direction. This triangle grows with the load increase and at the maximum, it reaches both sides of the sample (b). From that moment, a slanted zone is formed around the triangle (c). Then the triangular zone and the slanted zone grow together (d) and eventually the whole crack front is slanted and slightly curved (e).

DISCUSSION

It must be emphasized that KA60 specimens and MT760 panels exhibit exactly the same fracture aspect and then bring the same mechanisms into play. This justifies the future use of the KA60 specimen to model cracking of MT760 panels.

FE calculations have also been performed (not presented here). They show that the stress triaxiality ratio ($\sigma_{ii}/3\sigma_{eq}$) is highly geometry dependent. Ahead of the crack tip it can grow up to 1.6 in a KA60 or EV60 specimen when it is less than 0.6 in a TR6 specimen. As a high stress triaxiality ratio favours void growth, fracture mechanisms are related to it.

The comparison of the fracture surfaces obtained on smooth and differently notched specimens indicates two failure mechanisms. Voids are first initiated at intermetallic particles in both cases. At low stress triaxiality ratio, these voids tend to coalesce rapidly according to a “void sheet mechanism” [4] which creates smaller dimples in the inter-void ligaments. The failure of the specimens is essentially controlled by plastic instability (localization of plastic deformation into a shear band [5]). At higher stress triaxiality ratios, void growth is promoted and final rupture is caused by “internal necking” [6] between the large cavities initiated at intermetallics so that smaller dimples are not observed. The two failure mechanisms are schematized in figure 7. The first situation prevails in the slanted plane zone and the second in the crack initiation zone of severely notched specimens (triangular zone).

This underlines that fracture mechanism is geometry dependent and that a smooth tensile specimen would never capture all aspects of ductile rupture. The use of specimens which develop various stress triaxiality ratios is necessary.

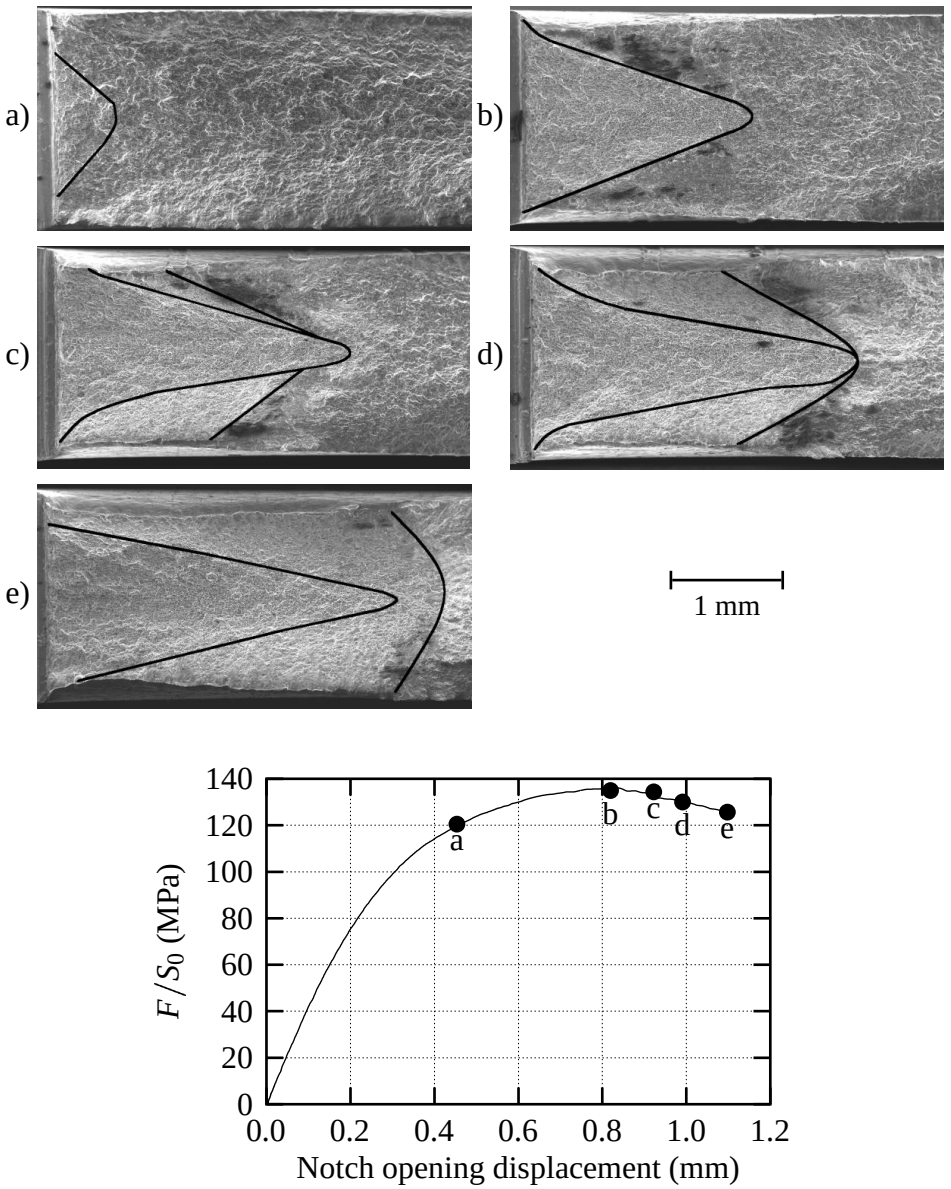

Figure 6: Failure initiation in a KA60 sample (interrupted tests) – F stands for the load and S_0 for the initial ligament surface

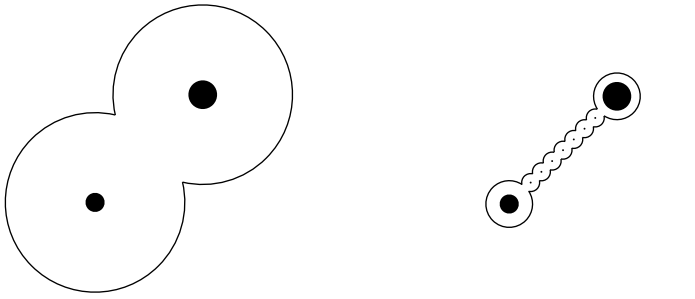

internal necking mechanism void sheet mechanism

Figure 7: The two failure mechanisms

CONCLUSION

The fracture mechanism of AA2024 thin sheets has been characterized. Two particular fracture modes were pointed out corresponding to different values of the stress triaxiality ratio. In the future, this should allow the development of a numerical model for ductile rupture.

ACKNOWLEDGEMENTS

The authors would like to thank Pechiney CRV for its interest in this work and financial support. Acknowledgements should also go to the French ministry of the economy, finance and industry for its financial support (ASA network).

REFERENCES

1. ASTM (1999) *Annual Book of* ASTM *Standards*, **03–01**, 509–521.
2. ASTM (1996) *Annual Book of* ASTM *Standards*, **02–02**, 1–7.
3. Besson, J., Brocks, W., Chabanet, O. and Steglich, D. (2001) *European Journal of Finite Elements*, (10), 401–415.
4. Garrison, W. M. and Moody, N. R. (1987) *J. Phys. Chem. Solids*, **48** (11), 1035–1074.
5. Rice, J. R. (1976). In: *Theoretical and Applied Mechanics*, Koiter, W. T. (Ed.), pp. 207–220. North-Holland Publishing Company, Amsterdam.
6. Thomason, P. F. (1985) *Acta Metallurgica*, **33** (6), 1079–1085.